

Soil carbon dioxide fluxes to atmosphere: the role of rainfall over CO2 transport

Isabelle Delsarte, Grégory Cohen, Marian Momtbrun, Patrick Höhener, Olivier Atteia

▶ **To cite this version:**

Isabelle Delsarte, Grégory Cohen, Marian Momtbrun, Patrick Höhener, Olivier Atteia. Soil carbon dioxide fluxes to atmosphere: the role of rainfall over CO2 transport. Applied Geochemistry, 2021, 127, pp.104854. 10.1016/j.apgeochem.2020.104854 . hal-03087039

HAL Id: hal-03087039
https://amu.hal.science/hal-03087039

Submitted on 5 Jan 2021

HAL is a multi-disciplinary open access archive for the deposit and dissemination of scientific research documents, whether they are published or not. The documents may come from teaching and research institutions in France or abroad, or from public or private research centers.

L'archive ouverte pluridisciplinaire **HAL**, est destinée au dépôt et à la diffusion de documents scientifiques de niveau recherche, publiés ou non, émanant des établissements d'enseignement et de recherche français ou étrangers, des laboratoires publics ou privés.

Soil carbon dioxide fluxes to atmosphere: the role of rainfall to control CO_2 transport

Isabelle DELSARTE[1*], Grégory COHEN[1], Marian MOMTBRUN[1], Patrick Höhener[2] and Olivier ATTEIA[1]

[1] EA 4592 G&E, Bordeaux INP, 1 allée F. Daguin, 33607 Pessac, France

[2] Aix-Marseille Université - CNRS, Laboratoire Chimie Environnement UMR 7376, 3 place Victor Hugo, 13331 Marseille, France

*isabelle.delsarte@bordeaux-inp.fr

Abstract

In order to observe the relationships between the temporal variations of CO_2 surface fluxes and the CO_2 soil gas transport in soil profile before and during rainfall events, two experiments were conducted in a controlled natural environment at different time periods. These experiments consisted in injecting pure CO_2 in a lysimeter at 160 cm depth and simulating heavy rainfall event at its surface for 2 weeks. During the whole experiments, CO_2 soil gas concentrations and surface fluxes were continuously monitored. These measurements showed that the flux measured through the flux chamber were consistent with the concentration profiles. During simulated rainfall events, the concentrations and fluxes showed a clear change linked to the presence of water on the top of the water profile. The results clearly show a significant decrease of CO_2 flux to atmosphere induced by rainfall infiltration and consequential wash-out of the CO_2 present in the soil.

Keywords: CO_2 concentration, soil CO_2 flux, rainfall, soil gas concentration and fluxes monitoring

1. Introduction

The soil is the interface between the different environmental compartments (lithosphere, the atmosphere…), where fluxes of water, particles and gas are constantly exchanged. Due to past and current human activities, the composition of these fluxes was significantly altered, that imposes a threat to the environment and human health. During the last decades, special attention has been paid to gas exchanges at the soil-atmosphere interface. Indeed, the need to understand and monitor gas fluxes is ubiquitous in many areas of human activity. For example, on the carbon capture and storage sites, the monitoring of CO_2 fluxes is necessary to detect and quantify eventual leakages to the environment (Bernardo and Vries, 2011; Beaubien et al., 2013; Schroder et al., 2016; Elío et al., 2016). Following landfill gas emissions across the surface of landfills is also essential. Indeed, the landfill gas is ranked as the third highest source of global anthropogenic methane emissions (Yang et al., 2015) and contributes also to large CO_2 emissions. Another example concerns the contaminated sites, where measurement soil gas fluxes are often required as part of human health risk assessment of the site or when implementing a risk-based corrective approach (Hers et al., 2004).

Gas flux at the soil-atmosphere interface, can be directly measured using flux chambers methods (Bornemann, 1920; Klenbusch, 1986). These techniques are based on the measurement of the compound concentration increase inside an open-bottom chamber set up on the soil surface. The gas flux is then calculated by relating the concentration increase during a given time to the chamber volume and the concerned soil surface area. Due to the low cost of this non-intrusive method which is easy to set up, it has been widely used (Cotel et al., 2015; Elío et al., 2016; Jassal et al., 2005; Matthias et al., 1980; Norman et al., 1997; Reinhart et al., 1992; Rochette and Hutchinson, 2005; Viveiros et al., 2008). Indeed, this technique allows to carry out *in situ* measurements quickly and on a large number of points compared to other techniques (Schroder et al., 2016).

However, due to the soil heterogeneity resulting from the spatial and temporal variability of the physico-chemical soil properties such as moisture, the instantaneous fluxes measured in practice do not allow to easily determine the long term transport of vapours to the atmosphere (Bekele et al., 2014). Several authors observed seasonal variations of gas surface fluxes or soil gas concentrations (Elío et al., 2013; Kim et al., 2019). Indeed, these researchers observed the dependence of CO_2 fluxes with soil moisture variations which are likely to govern soil gas transport processes. Petersen et al. (1996) and Choi et al. (2005) observed that trichloroethene (TCE) gas-phase diffusive fluxes at soil surface were also sensitive to soil-water content modifications. Moisture content in the subsurface modifies the pore volume available for gas transport (Risk et al., 2002; Tillman and Smith, 2004; Palaia et al., 2018). Moisture content impacts the transport of gas phase in the soil by modifying soil tortuosity as well as the effective diffusivity and the dissolved quantity of the concerned compound in the aqueous phase (Conant et al., 1996; Hers et al., 2000; Jassal et al., 2005). In the literature, there is still an ongoing discussion about the different formulae used to link soil water content to the effective tortuosity (Hers et al., 2000; Werner et al., 2004). The heterogeneous distribution of soil moisture content has also a direct effect on subsurface gas concentration profile (Shen et al., 2013). Wetter soil layers could therefore have different effects such as reducing the gas diffusion from the source to the atmosphere or, conversely, increasing surface fluxes. It was also shown that rainfall duration, intensity, frequency and spatial variability has direct influence on gas fluxes (Fa et al., 2015; Lelli and Raco, 2017; Ma et al., 2012; Seo et al., 2020; Tommasone Pascale et al., 2015). In their study, Viveiros et al. (2008) showed that depending on the intensity of the rainfall, the soil CO_2 fluxes are different. Tommasone Pascale et al. (2015) observed the influence of rainfall events on soil radon (^{222}Rn) concentration and concluded that time evolution of soil ^{222}Rn activities are markedly dependent on the rainfall history of the site.

While there is a general agreement on the importance of soil water content, there has been, to our knowledge, limited quantitative analysis related to its influence (Hers et al., 2000; Oh et al., 2019; Shen et al., 2013). Even if some field and / or numerical studies have considered some temporal effects on soil gas transport, a full explanation of the influence of rainfall events on soil gas concentrations and fluxes is still not available (Viveiros et al., 2008; Lewicki et al., 2009; Shen et al., 2012). However, understanding how these short and/or long-term variations modify soil gas transport processes is of major importance for precisely quantify long term gas fluxes at monitoring sites.

Therefore, the main objective of this study is to understand the relationships between the temporal variations of gas surface fluxes and the soil gas transport in soil profile before and during rainfall events. To this end, two experiments were conducted in a controlled natural environment. These experiments consisted in injecting pure CO_2 in a lysimeter and simulating rainfall event at its surface. During the whole experiments, CO_2 soil gas concentrations and surface fluxes were continuously monitored. The impact of natural rainfall events of different intensities and frequencies on CO_2 fluxes at the soil-atmosphere interface were also observed.

2. Materials and methods

2.1.Lysimeter description

The experiments were conducted in a lysimeter, a controlled natural environment (Figure 1). This lysimeter was set up in August 2014. Soil digging was conducted thanks to a mechanical shovel which removed and separated sequentially 50 cm depth soils layers until 1.85 m depth. The retention tank ($l \times w \times h$ = 1.35 x 1.35 x 0.8 m) was then set-up. At the bottom of the tank, a grid was added allowing an easier water recovery. Moreover, a gooseneck system, connected to the bottom of the retention tank allows the control of the piezometric level and the quantification of outflowing water. After the set-up of the retention tank, the soil was manually put back in place backward in order to respect as much as possible the original soil

configuration. Each soil layer of 10 cm height was compacted. In the centre of lysimeter, six gas probes were set up during this backfill, placing them at specific depths (0.4, 0.8, 1.0, 1.2, 1.4 and 1.6 m depth) (Figure 1). To avoid vertical preferential paths, their tubes were placed in the ground horizontally until the manhole. Thus, the soil removed during the lysimeter installation was returned to respect as much as possible its initial structure. The soil matrix is an alluvial sand from the Aquitaine basin (France). Moreover, the soil does not contain calcite (<1%) over the entire vertical profile of the lysimeter and the CEC capacity varies from 15 $mmol_c/kg$ at 20 cm to 1-2 at 1 m depth.

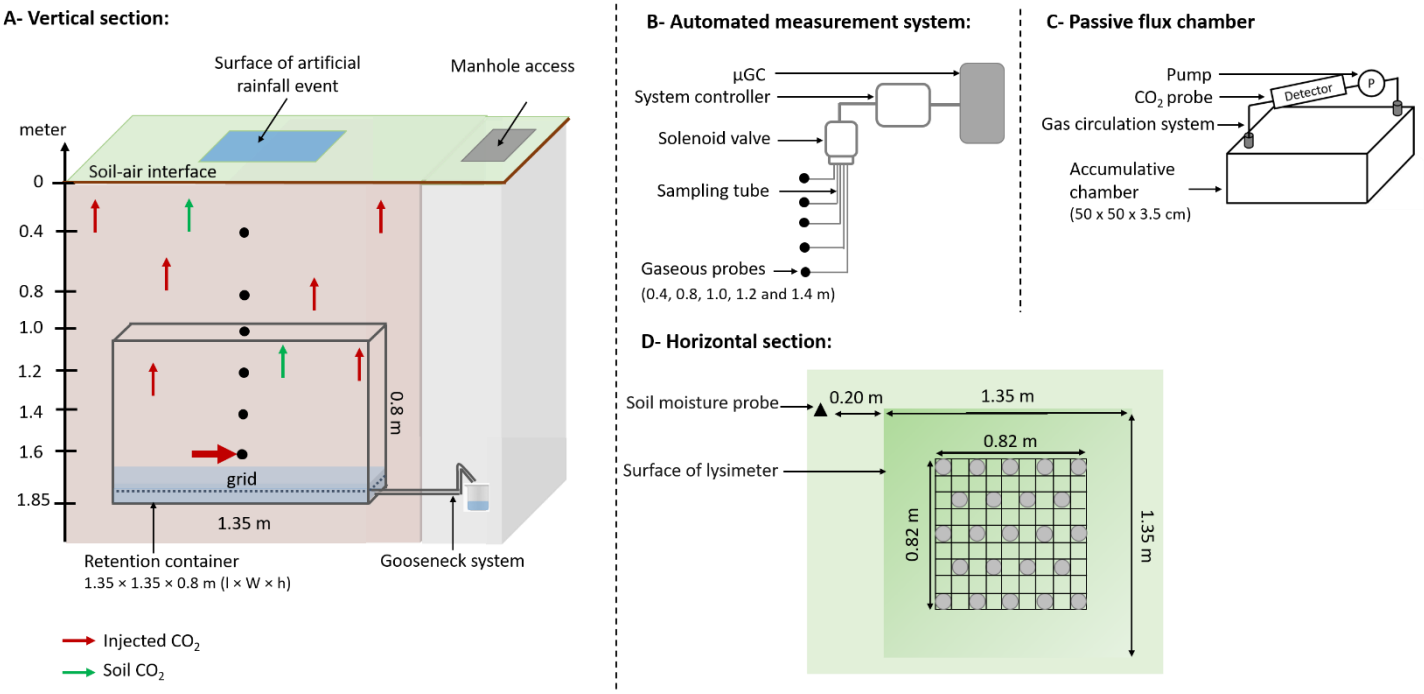


Figure 1. General description of the lysimeter. A- Vertical section of the lysimeter: a grid rested on the bottom of the tank and allowed the porous medium to be separated from the water. The black dots represent the location of the gas probes. B- Automated measurement system for continuous monitoring of CO_2 concentrations in the soil. C- Schematic of passive flux chamber used to determine surfaces fluxes. D- Horizontal section of the lysimeter: the blue and grey dots represents the location of the piezometer and the tubes used for artificial the rainfall event, respectively.

2.2.Hydrological properties of porous media

2.2.1. Determination of soil porosity and water content by soil coring

The initial water content, the residual water saturation and the porosity of the porous medium were experimentally determined. Soil cores were taken from the experimental plot next to the lysimeter at 0.2, 0.5 and 1.0 m depth. The sampling tool consists in a sampling tube on which is added a corer (S x L: 11.95 x 14.8 cm^2). A pilot hole is previously made with a manual auger to the desired depth. The tube is then driven into the ground either directly or with a sledgehammer. Soil cores were first slowly saturated with tap water for 24 h before being placed in the oven at 105°C for 24 h (Wilke, 2005). At every step, soil cores were weighted.

2.2.2. Transient water content measurement

Soil moisture content was determined by using moisture probes (120 cm; Drill & Drop Probe, SDI-12, Sentek) composed by ten moisture sensors. Thus, soil moisture was measured every 10 cm from 7 to 97 cm depth. To avoid preferential gas flow and damage of gas sample probes, this probe was set up 20 cm next to the lysimeter (Figure 1). The soil matrix at this emplacement is the same as the one inside the lysimeter. The soil moisture probes were calibrated *in situ* by an analysis of their temporal signal variations with respect to the cumulative amount of water infiltrated during the artificial rainfall event.

2.3.CO_2 soil gas concentration measurements

CO_2 soil gas concentrations were continuously monitored with the use of a custom automated system. This automated system is composed of a micro-GC (CP-4900, Varian Inc.), a system controller (M3 Essential extensibles, Crouzet) and a solenoid valve (EMHMA-CE, Vici Valco) directly connected to the five soil gas probes (0.4, 0.8, 1.0, 1.2 and 1.4 m depth) (Figure 1). The micro-GC is equipped with a PPQ column to separate CO_2. The general relative uncertainty for the quantification of CO_2 with this method is less than 5%. Tubes of 2.50 m

with an inner diameter of 0.5 mm were used to connect each gas probe to the automated system. For each analysis, a gas sample of 70 mL was collected from the soil by micro-GC pumping system. The dead volumes of the gas tubes were taken under consideration to determine the optimal sampling volume.

2.4.Gas flux monitoring at the soil surface using a flux chamber

A Passive Flux Chamber (PFC) (50 x 50 x 3.5 cm (L × W × H)) was used to monitor CO_2 gas fluxes at the centre of the lysimeter surface (Figure 1). A sealed pumping system with a flowrate of about 500 mL min^{-1} allows gas circulation from the accumulation chamber to the detector and its homogenization inside the PFC. The CO_2 concentrations were measured with a CO_2 probe (GMT222 Vaisala) placed in the PFC gas circulation system. To correct the CO_2 probe values, an intercomparison with the micro-GC was realized. This step was realized on several CO_2 concentrations (Information is available in the Supplementary information).

The soil surface CO_2 gas fluxes (F_{CO2} in g m^{-2} min^{-1}) were calculated during the transient state of gas transfer in the flux chamber headspace as follows (Matthias et al. 1980):

$$F_{CO2} = \frac{V_{ch}}{A_{ch}} \times \frac{dC}{dt} \quad (1)$$

Where dC (g m^{-3}) is the variation of the CO_2 vapour concentration in the chamber during dt (min), V_{ch} (m^3) is the net volume of the chamber, and A_{ch} (m^2) the covered soil surface area.

Based on the principle of gas accumulation within the chamber, the initial slope of the measured gas concentration-time curve is generally used to quantify the time derivative of Eq. (1) (Cotel et al. 2015).

Uncertainties in the experimental CO_2 mass fluxes measured with this flux chamber were calculated according to the method used by Cotel et al. (2015). Thus, uncertainties in the flux measurements were determined using a total derivative expansion for correlated variables of F_{CO2}:

$$\frac{\Delta F_{CO_2}}{F_{CO_2}} = \sqrt{\left(\frac{\Delta(dC/dt)}{dC/dt}\right)^2 + \left(\frac{\Delta V_{ch}}{V_{ch}}\right)^2 + \left(\frac{\Delta A_{ch}}{A_{ch}}\right)^2} \quad (2)$$

Considering uncertainties of 5%, 4% and 8% for CO_2 detector measurements, PFC section and volume, respectively, the total uncertainty in the measured fluxes is about 10.25%.

2.5.Experimental conditions

The same experiment was realized at two different times of the year, in February and October 2019. The timeline of both experiments is presented in Figure 2. For each experiment, the CO_2 injection began at day 0. When the CO_2 concentration gradient was stabilized, an artificial rainfall event was realized at 8.6 d for the 1st experiment and at 6 d for the second (cf. 2.5.2). For the 2nd experiment, a natural rainfall event followed the artificial one at 9 d. During the experiments, the atmospheric pressure varied between 1018 and 1031 hPa for the 1st experiment and between 992 and 1023 hPa for the 2nd experiment.

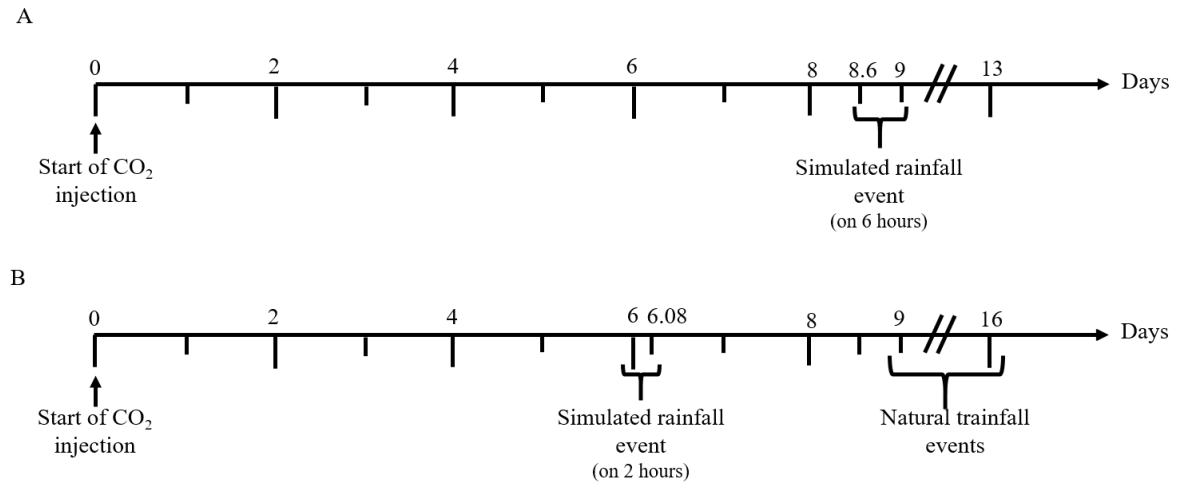


Figure 2. Timelines of the experiment realized in February 2019 (A) and in October 2019 (B).

2.5.1. Gas injection conditions

The gas injection was conducted with a bottle of CO_2 (99.7% Air Liquide) equipped with a flow controller set at about 0.3 $L.min^{-1}$. The gas was injected inside the retention tank at 160 cm depth of the lysimeter for 2 weeks.

171 2.5.2. Artificial rainfall event

172 For the two experiments, an intense rainfall event of about 100 mm of tap water was
173 simulated during respectively 6 h and 2 h. The rainfall event was conducted in the centre of the
174 lysimeter over a surface of 0.82 × 0.82 m (0.67 m^2) leading to a total of 69 L. On this surface,
175 23 tubes (inner diameter: 8 cm; H: 15 cm) were placed regularly on a regular mesh (Figure 1)
176 and pressed 2 cm deep. These tubes allowed the homogeneous injection of tap water in soil (12
177 x 250 mL / tube). The water was recovered at the outlet of the lysimeter through the gooseneck
178 system (Figure 1). During the 2nd experiment, the same amount of water was injected in the
179 centre of the lysimeter and an equivalent artificial rainfall event was also realized around the
180 moisture probe. The rainfall event around the latter was conducted over a surface of 0.63 x
181 0.63 m leading to a total of 42 L. Given the proximity of the probe to the lysimeter,
182 approximately 50% of the quantity of water injected could be collected at the outlet of the
183 lysimeter, *i*.e. the equivalent of 90 L.

184 2.6.Calculation of the CO_2 mass balance

185 The domain considered for determining the approximate mass balance is the surface
186 covered by the artificial rainfall event (0.672 m^2) across a depth of 80 cm, equivalent to a
187 volume of 538 L. This domain is divided over depth in 16 equal subdomains (l × w × h = 82 x
188 82 x 5 cm). Each subdomain was characterised by the porosity, soil moisture content, gas phase
189 volume as well as CO_2 soil concentrations in aqueous and gaseous phase.

190 According to porosities determined by soil coring method, a porosity of 0.33 was
191 considered for the subdomains located between 0 to 0.5 m depth and 0.29 for the others located
192 between 0.5 to 0.8 m depth. Soil moisture content of each subdomains was estimated based on
193 soil moisture profile data allowing to calculated water phase volume ($V_{aqueous\ \mathrm{phase}}$):

194 $$V_{aqueous\ phase} = \theta_{water} \times V_{subdomain} \quad (3)$$

195 Where Θ_{water} (-) is the volumetric soil water content and $V_{subdomain}$ (L) is the volume of the
196 subdomain.

197 The gas phase volume was then calculated as follows:

198 $$V_{gaseous\ phase} = (\theta - \theta_{water}) \times V_{subdomain} \quad (4)$$

199 Where Θ (-) is the total connected porosity.

200 CO_2 mass in the gaseous phase in each subdomain was determined based on CO_2 profiles
201 data (Figure 5) and linear interpolation method. Assuming that in the soil the equilibrium
202 between aqueous and gaseous phase was instantaneous, Henry's law was used to calculate the
203 CO_2 mass in the aqueous phase ($m_{\text{aqueous phase}}$):

204 $$m_{aqueous\ phase} = (C_{gaseous\ phase} \times H^{cc}) \times V_{aqueous\ phase} \quad (5)$$

205 Where, H^{cc} is the dimensionless Henry solubility (C_a/C_g). According to Sander et al. (2011) the
206 H^{cc} value is 0.818 at 25°C.

207 However, the H^{cc} value can change according to the buffering capacity (or alkalinity) of
208 soil water which is the water capacity for solutes it contains to react with and neutralize acid.
209 Thus, in contact with water, H_2O (l) and CO_2 (g) form a carbonic acid molecule H_2CO_3 (aq)
210 according to the carbonation reaction:

211 $$CO_{2\,(g)} + H_2O_{\,(l)} \leftrightarrow H_2CO_3{}^*_{\,(aq)}$$

212 Where H_2CO_3* represents the total concentration of dissolved CO_2 and H_2CO_3.

213 As H_2CO_3 (aq) is an acid, it reacts to form a bicarbonate ion HCO_3^- (aq) and a solvated
214 proton H_3O^+ (aq):

215 $$H_2CO_3{}^*_{\,(aq)} + H_2O_{\,(l)} \leftrightarrow HCO_3^-{}_{(aq)} + H_3O^+_{\,(aq)}$$

216 Then:

217 $$HCO_3^-{}_{(aq)} + H_2O_{\,(l)} \leftrightarrow CO_3^{2-}{}_{(aq)} + H_3O^+_{\,(aq)}$$

The previous reactions increase the apparent solubility of CO_2. These dissolutions can also be increased in presence of calcite. However, the Bernard calcimeter method showed that the level of calcite in the soil studied was inferior to the quantification level (0.1%) (Rodier, 1976). Thus, from the alkalinity, pH and CO_2 added in the media, an apparent Henry constant (H_{app}^{cc}) can be calculated. Before and during the CO_2 injection (at steady state), alkalinity measurements were realized by titration method (Table 1) on the water recovered at the outlet of the lysimeter (Rodier, 1976). Alkalinity at 0.4 m and 0.8 m was estimated based on CO_2 concentration profile at steady state (Figure 5) and alkalinity in the outflowing water using a linear interpolation (Table 1). According to this method, the average value of H_{app}^{cc} estimated is 1.151 at 15°C.

Table 1. Parameters of the water recovered at the outlet of the lysimeter before and during the CO_2 injection at steady state.

Experiment		at 0 d	At steady state		
Depth (m)		1.85	1.85	0.8	0.4
Soil	CO_2 gas concentration (% Vol CO_2)	0.30	99.70	20.73	4.55
	CO_2 gas concentration added[a]	/	99.40	20.43	4.25
Aqueous phase	pH	7.39		6.41	
	Alkalinity (mol L^{-1})	0.0034	0.0256	/	/
	H_2CO_3 concentration (mol L^{-1})[a]	0.0004	0.0259	/	/
	HCO_3^- concentration added (mol L^{-1})[b]	/	0.0222[a]	0.0046	0.0009
	H_2CO_3 concentration added (mol L^{-1})[c]	/	0.0255[b]	0.0052	0.0011

[a] 10^(pKa x log([HCO_3^-]) – pH) with pKa = 6.415 at 15°C

[b] [HCO_3^-] added = ([HCO_3^-] at steady state - [HCO_3^-] at 0 d) x% CO_2 gas concentration added

[c] [H_2CO_3*] added = ([H_2CO_3*] at steady state - [H_2CO_3*] at 0 d) x% CO_2 gas concentration added

234 3. Results

235 3.1.Artificial rainfall event monitoring

236 Figure 3 shows the evolution of soil moisture content as a function of depth at different
237 periods: before and during the artificial rainfall event. For the 2nd experiment, the initial soil
238 moisture content was different than for the 1st experiment (Figure 3).

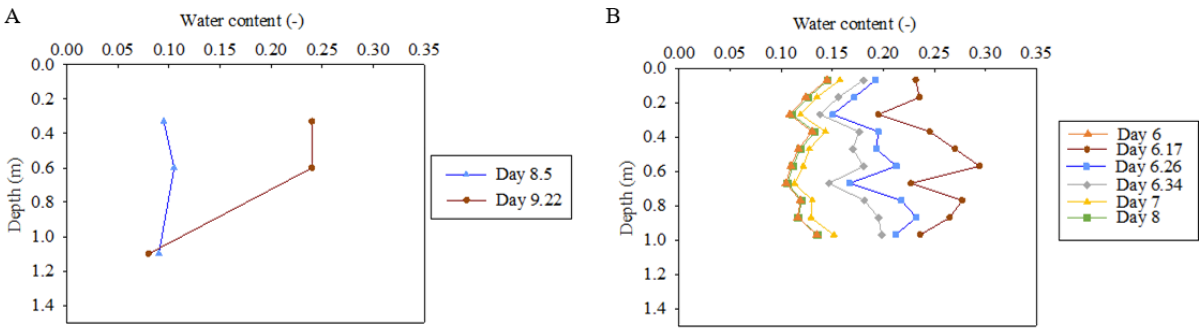


Figure 3. Spatial variation along vertical profile for soil moisture during and after the artificial rainfall event in February 2019 (A) and October 2019 (B) experiments.

239

240 Indeed, initial moisture content was in average of 0.097 for the February experiment
241 and 0.12 for the 2nd experiment. Even if, water content varies in function of the depth, a
242 consistent evolution of the profiles was observed during and after the rainfall event.

243 Figure 4 presents the cumulative outflow of water recovered at the outlet of the
244 lysimeter. Two days after the artificial rainfall event, only 50% of the water amount injected
245 was collected for the 1st experiment while this value was 92% for the 2nd experiment for the
246 same duration. This difference may be linked to initial soil moisture content which was higher
247 during the 2nd experiment (Figure 3).

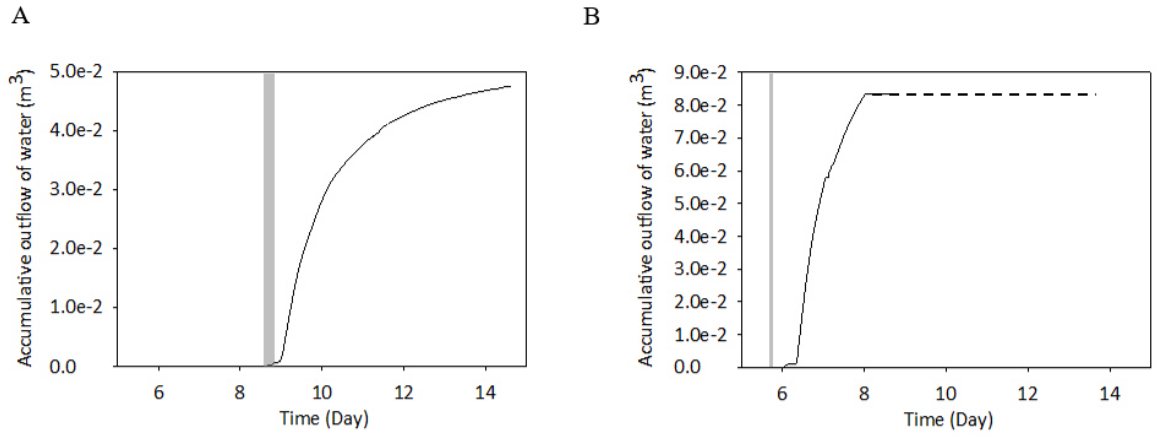


Figure 4. Cumulative outflow obtained during and after the artificial rainfall event in February 2019 (A) and October 2019 (B). The artificial rainfall events are highlighted with a grey area. The dotted lines indicate a data acquisition problem.

248

249 3.2. Soil CO_2 concentrations

250 Figure 5 presents the evolution of CO_2 soil gas concentrations as a function of depth at
251 different periods during the gas injection, until CO_2 profile stabilization. Measures were
252 realized before the CO_2 injection for baseline data. The CO_2 profiles obtained were like that
253 presented on Figure 5 at day 0 with a low CO_2 content ≈ 0.3 vol %. During the injection, CO_2
254 content between 0.4 and 1.4 m depth respectively increased until 5 and de making the CO_2
255 produced by the soil respiration negligible.

256 The CO_2 concentration at 0 m depth corresponds to the atmospheric concentration of
257 CO_2. For the first experiment, the CO_2 stabilization in the soil occurred about 4 days after the
258 injection began (Figure 5-A). For the second experiment, the stabilization occurred later, about
259 5-6 days after the injection started. Indeed, even if the overall profile seems to be stable at day
260 4, CO_2 concentration at 0.4 m depth still varied after day 4 in the 2nd injection (Figure 5-B).
261 Moreover, during the injection, a change of slope at 0.8 m depth was observed. Due to its
262 density, CO_2 gas (1.83 instead of 1.21 kg m^{-3} for air), may have accumulated in the lysimeter,
263 *i.e.* between 1.05 and 1.85 m depth, and the concentrations at 0.8 m may be influenced by dense
264 CO_2 flowing laterally from the lysimeter to the surrounding soil. This may explain the change

of CO_2 concentration slope observed at 0.8 and 0.4 m. Indeed, compared to diffusion, the density effect can be neglected only for very low concentrations. Thus, the interpretation of obtained results focused above all on the first 0.8 m of the lysimeter.

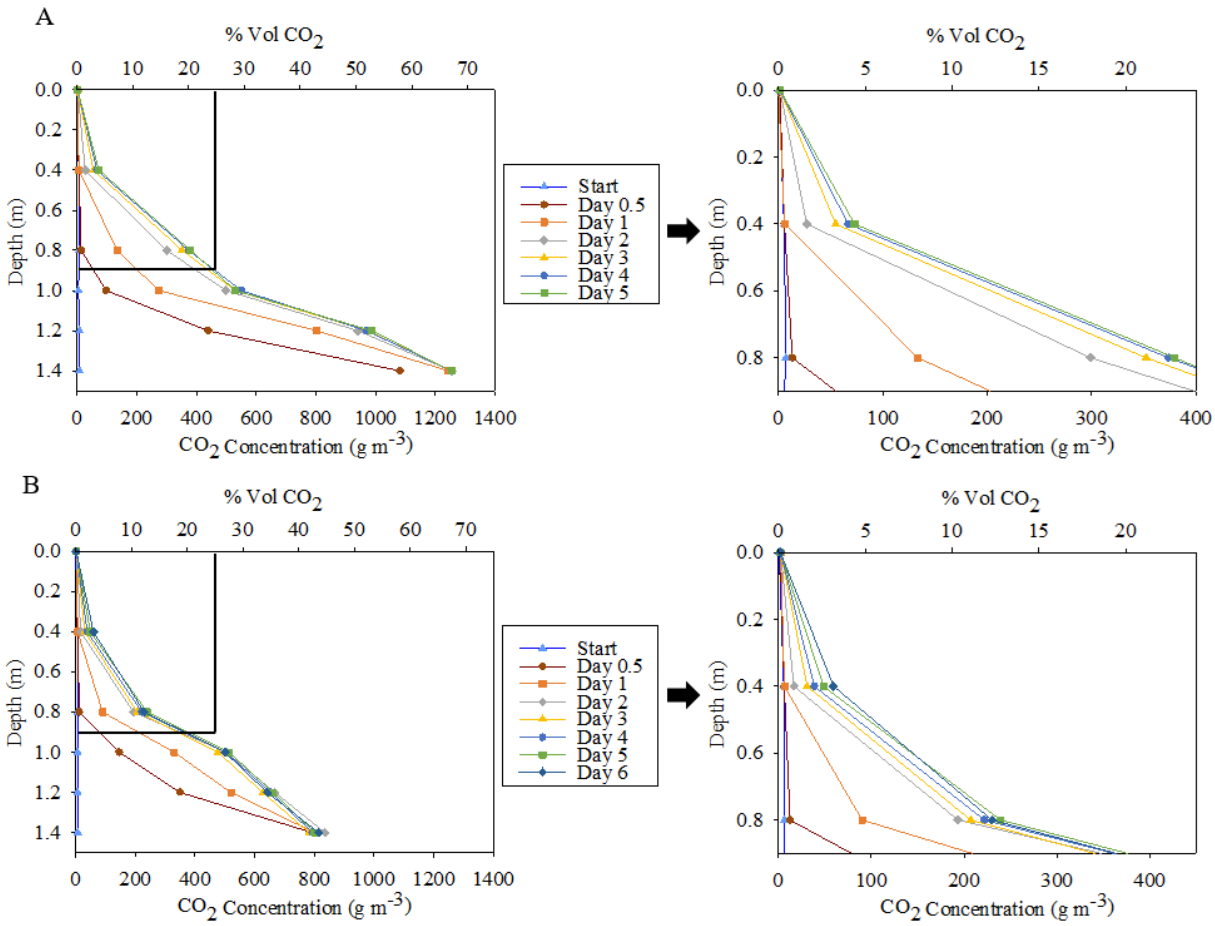


Figure 5. Evolution of CO_2 concentration profile at different period during the CO_2 injection in February 2019 (A) and in October 2019 (B). For A and B, the figure on the right is the inset of the figure on the left.

The temporal evolution of CO_2 soil gas concentrations is presented in Figure 6. In the left part of each graph, the increase of CO_2 soil concentrations is clearly observed during the beginning of the injection. The CO_2 gas concentrations at 0.4 and 0.8 m depth respectively increased to 80 and 380 g m^{-3} for the February experiment and to 50 and 230 g m^{-3} for the 2nd experiment. The grey part of graphs related to rainfall events will be described below.

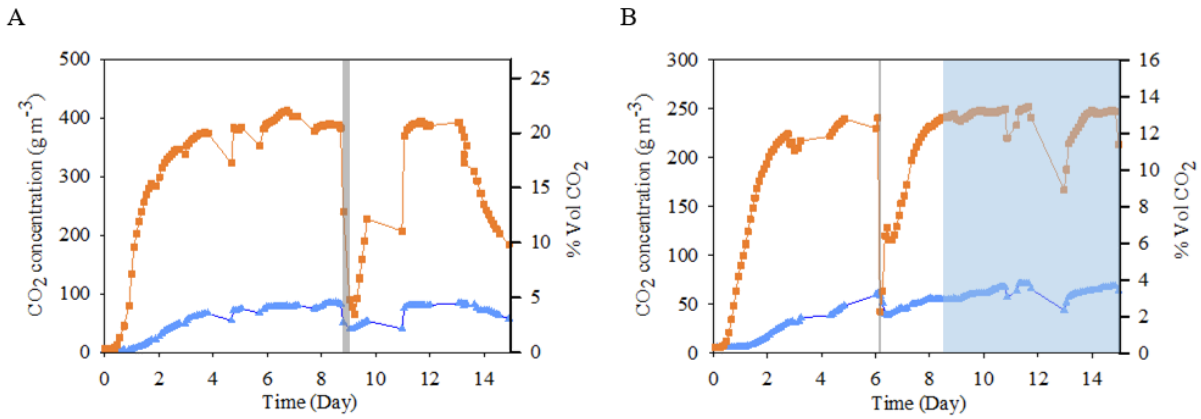


Figure 6. Times series for CO_2 soil gas concentrations measured at 0.4 (blue dots) and 0.8 m (orange dots) depth, in the centre of the lysimeter during the CO_2 injection in February 2019 (A) and in October 2019 (B). The artificial and natural rainfall events are underlined by a grey and blue area, respectively.

After the artificial rainfall event, the CO_2 profiles showed a significant modification linked to the presence of water at the top of the lysimeter. In fact, a clear decrease of CO_2 gas concentrations was observed, especially at 0.8 m depth (Figure 6 and 7). During the 1st experiment, the CO_2 concentration at this depth decreased rapidly from 388 to 65 g m^{-3}. This minimum CO_2 concentration was measured 14 h after the beginning of the rainfall event and represents a 5.9-fold decrease (Figure 7). Then, CO_2 concentrations increased and reached their previous concentrations after two days. For the 2nd experiment, the CO_2 minimum concentration was reached faster than for the 1st experiment. Indeed, the CO_2 concentration at this depth decreased rapidly from 240 to 42 g m^{-3}. This minimum CO_2 concentration was measured 4 h after the beginning of the rainfall event and represents a 5.6-fold decrease. Then, the CO_2 profiles returned to the steady state after 2.75 and 2 days for 1st and 2nd experiment, respectively (Figure 7).

The CO_2 gas concentrations variations can be analysed in relation with soil moisture content change for the second rainfall event (Figure 3). The highest soil moisture contents were observed at 6.17 d when the CO_2 gas concentration at 0.8 m depth was the lowest. Moreover,

the moisture content profile turned back to steady state after 2 days as for CO_2 concentration profile (Figure 3 and 7).

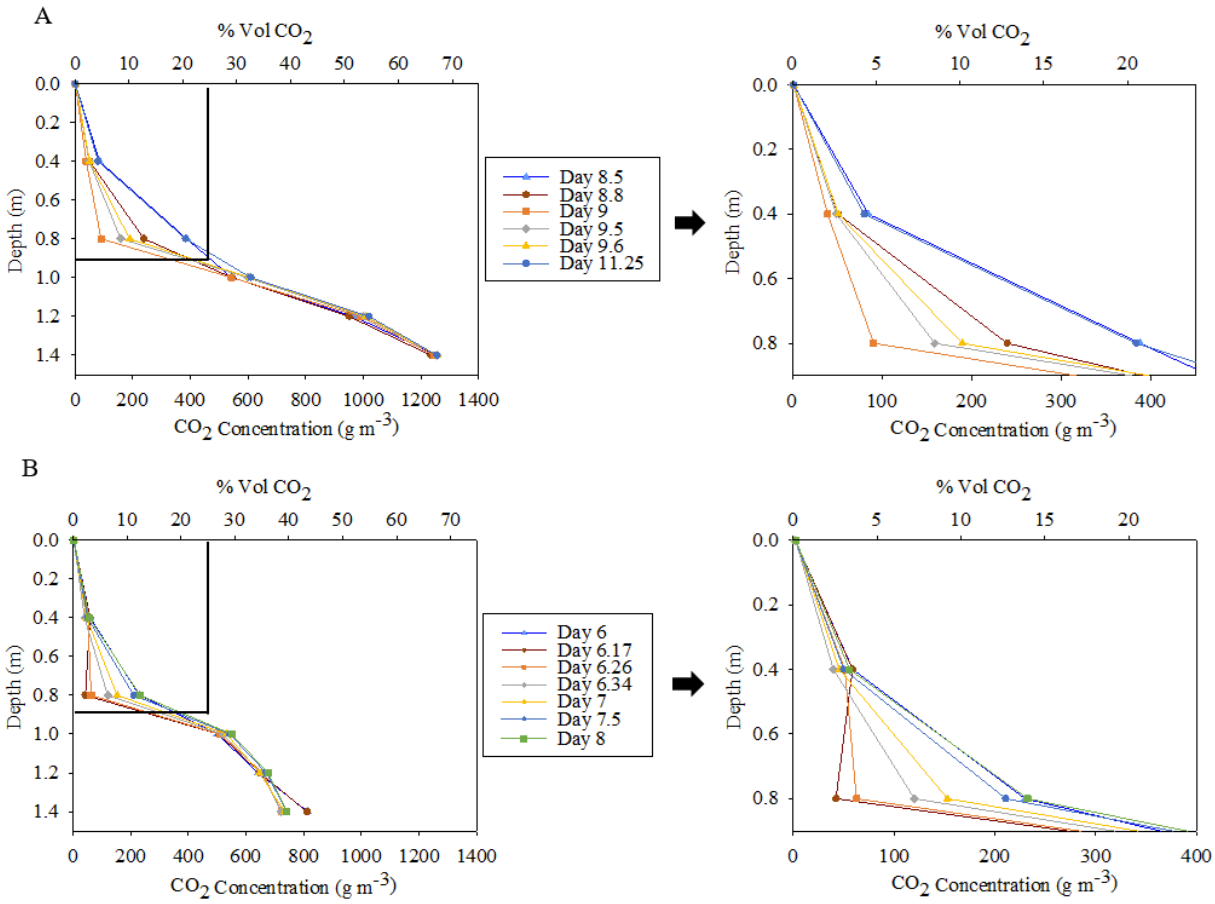


Figure 7. Evolution of CO_2 concentration profile at different period after the rainfall event, at 9 d for February 2019 (A) and at 6.08 d for October 2019 (B). For A and B, the figure on the right is the inset of the figure on the left.

3.3. CO_2 soil surface fluxes

The temporal evolution of CO_2 fluxes at lysimeter surface are presented in Figure 8. For the 1st experiment, the measured CO_2 fluxes increased until a stabilization around 35 mg m^{-2} min^{-1} which occurred about 5 days after injection began. For the 2nd experiment, the measured CO_2 fluxes increase until about 40 mg m^{-2} min^{-1}. The fluxes measured across the surface were greatly inferior compared to the injected CO_2 flux because part of injected CO_2 escapes laterally and another part accumulates at depth.

After the artificial rainfall events, a significant decrease of CO_2 fluxes was noticed for both experiments. They dropped from 35 to below 10, and from 40 to 1 mg m^{-2} min^{-1} for 1st and 2nd experiment (Figure 8), respectively. After these events, the CO_2 fluxes previously obtained at steady state were not reached again, while the soil CO_2 concentrations reached back their original values (Figure 7).

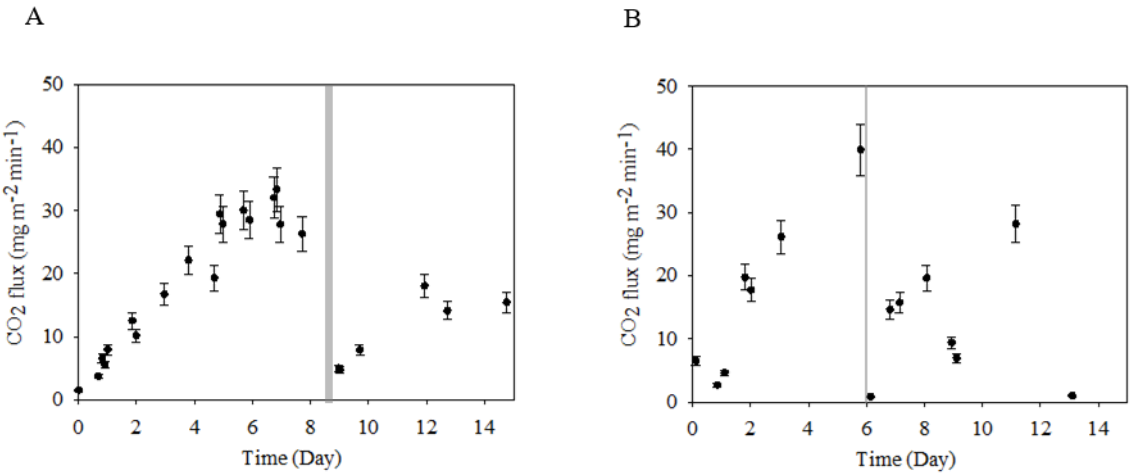


Figure 8. Times series of CO_2 soil surface fluxes, in the center of the lysimeter during the CO_2 injection in February 2019 (A) and in October 2019 (B). The artificial rainfall events are highlighted with a grey area.

3.4. CO_2 mass balance

To understand the influence of rainfall events on surface CO_2 gas fluxes, an approximate mass balance was calculated for both experiments. This mass balance is based on CO_2 profiles data obtained at the steady state (at 8.5 d and 6 d for event 1 and 2, respectively) and after the artificial rainfall events (at 9.22 d for event 1 and at 6.17 and 6.34 d for event 2) (Table 2), considering the surface covered by the artificial rainfall event (0.67 m^2) across a depth of 80 cm. CO_2 mass in the aqueous phase was calculated with a standard H^{cc} value (Sander et al., 2011) and H_{app}^{cc} determined according to the alkalinity data.

316 Table 2. Estimated mass balance between the end of steady state of CO_2 profile and the end of
317 the artificial rainfall event.

Zone characteristics	
Area considered (m^2)	0.672
Investigated volume (0 to 0.8 m depth) (L)	538
Pore volume [a] (0 to 0.8 m depth) (L)	170.18

Media	Experiment	1st		2nd		
		At steady state	After artificial rainfall event	At steady state	After artificial rainfall event	
		at 8.5 d	at 9.22 d	at 6 d	at 6.17 d	at 6.34 d
Soil	Volume of soil gaseous phase (L)	118.31	46.46	105.59	33.65	89.57
	Volume of the soil aqueous phase (L)	51.87	123.72	64.59	136.53	80.61
	CO_2 mass in the gaseous phase (g)	16.55	1.82	9.99	1.3	4.16
	CO_2 mass in the aqueous phase with H^{cc} = 0.818 (g)	6.70	3.92	4.97	4.96	4.17
	CO_2 mass in the aqueous phase with H^{cc} = 1.151 (g)	9.43	5.52	6.99	6.98	5.86
Interface soil/air	CO_2 Flux (mg m^{-2} min^{-1})	29.4 ± 3.8	5.69 ± 0.74	39.9 ± 5.19	0.79 ± 0.1	4.8 ± 0.62
	CO_2 flow (g min^{-1})	0.020	0.004	0.027	0.0005	0.003
	Mass Balance c	1st		2nd		
		9.22 d - 8.5 d		6.17 d - 6 d	6.34 d -6.17 d	
Soil	Δ CO_2 mass in the gaseous phase (g)	-14.73		-8.69	2.86	
	Δ CO_2 mass in the aqueous phase with H^{cc} = 0.818 (g)	-2.78		-0.01	-0.79	
	Δ CO_2 mass in the aqueous phase with H^{cc} = 1.151 (g)	-3.91		-0.01	-1.12	
Interface soil/air	Δ CO_2 mass (g)	16.59 ± 2.16		6.48 ± 0.84	0.66 ± 0.9	

318 [a] Determined according to CO_2 concentration profile at steady state
319 [b] Determined according to CO_2 concentration profile after the artificial rainfall event
320

321 During the 1st experiment, at steady state (8.5 d), the considered soil volume contained
322 between 23.25 and 29.95 g of CO_2 with 16.55 g gaseous phase and between 6.70 and 13.40 g
323 in aqueous phase. After the artificial rainfall event, at 9.22 d, the total CO_2 mass contained in
324 considered soil volume decreased drastically. Indeed, the soil only contained between 5.74 and
325 9.61 g (about 3.6 times less than at steady state) with 1.82 g gaseous phase and between
326 3.92 and 7.79 g in aqueous phase. According to this mass balance, the mass of CO_2 lost in the
327 gas phase between 8.5 and 9.22 d would have been moved to the atmosphere at the top of the
328 investigated volume. In fact, according to CO_2 flux measurements, the CO_2 amount emitted at
329 the soil/air interface during this period was 16.59 ± 2.16 g, corresponding rather well to the
330 mass of CO_2 lost in the gas phase of about 14.73 g (Table 2). Concerning, the CO_2 amount in
331 aqueous phase between these two states, it did not increase significantly, even if the quantity of

water injected at the soil surface (about 69 L) was localised in the investigated volume. Indeed, the volume of the soil aqueous phase was 51.9 L at 8.5 d and 123.7 L at 9.22 d.

The same observations were done for the 2nd experiment. Indeed, CO_2 mass decreased after the artificial rainfall event (6.17 d) by a factor of 2.1. The CO_2 amount in aqueous phase did not significantly vary. The mass balance also shows that the mass of CO_2 lost in the gas phase between 6.0 and 6.17 days is equivalent to the one lost at the top of the lysimeter. After day 6.34 of this 2nd experiment, a return at steady state conditions is observed (11 d) (Figure 7). Indeed, the water added begun to flow out of the investigated volume and the CO_2 mass in the gaseous phase begun to increase. A decrease, between 0.79 and 1.57 g of CO_2 in the aqueous phase is observed (Table 2).

3.5.Influence of natural rainfall events

The temporal evolution of precipitations and soil moisture content after the 2nd rainfall event are presented in Figure 9. The rainfall events modify directly soil moisture content even during a light and short-term rain. However, the depth of soil moisture modification varies according to the rainfall intensity and duration. For example, during the light and short-term rains between 20 and 22 d, a little increase of soil moisture could be only observed at 0.07 m depth whereas during the light and longer-term rainfall events (18 d - 19 d), the water contents were modified at 0.07 and 0.37 m depth (Figure 9-C and D). During the heavy natural rainfall events highlighted in blue (Figure 9-C), soil moisture increased at every depth.

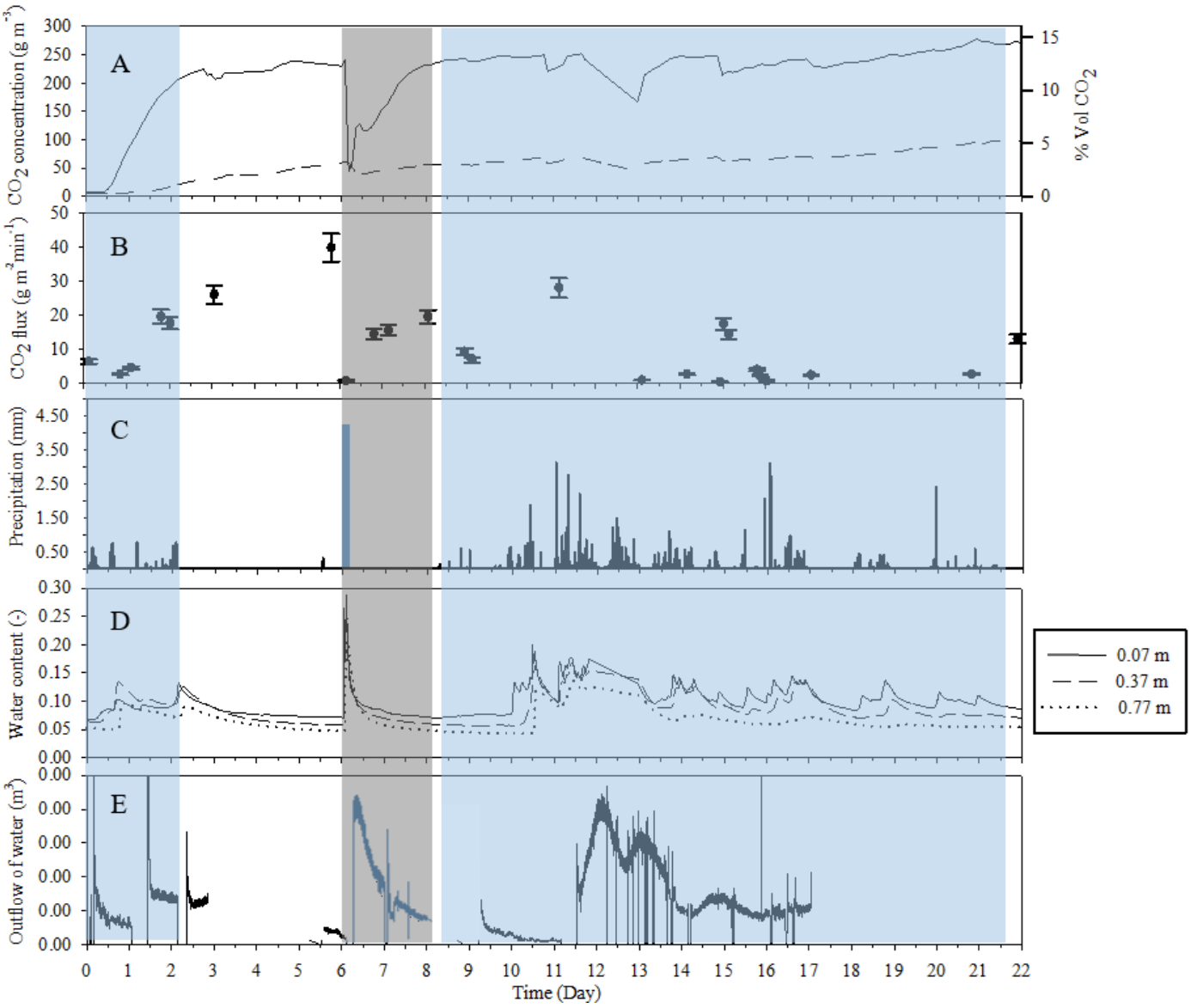


Figure 9. For the october experiment, times series of (A) CO_2 soil gas concentrations measured at 0.4 (solid line) and 0.8 m (short dash) depth, (B) CO_2 soil surface fluxes, in the centre of the lysimeter, (C) precipitation, the heavy rain are highlighted, (D) relative soil moisture at 0.07, 0.37 and 0.77 m depth and (E) outflow of water recorded during natural rainfall events from 8 d to 22 d of the October experiment. The data obtained after the artificial rainfall event are highlighted in grey.

357

358 The evolution of CO_2 soil gas concentrations and CO_2 fluxes at lysimeter surface during
359 natural rainfall events are also shown in Figure 9. The evolution of CO_2 fluxes showed a
360 relationship with the relative soil moisture (Figure 9-B, C and D) The CO_2 fluxes can be
361 analysed between day 13 and 17 where enough measurements could be done (Figure 9-B).
362 Between day 13 and 15, the effect of the heavy rainfall identified through the high water content

363 seem to lead to very low values of CO_2 fluxes (below 1 mg m^{-2} min^{-1}), despite the still high CO_2
364 concentrations in the soil. These values are even lower than the one observed during or after
365 the artificial event. This may be linked to the higher water content than during the artificial
366 event period. During a short period, at day 15, some values of significant fluxes, close to the
367 one after the artificial rainfall event, are observed (≈ 17.5 mg m^{-2} min^{-1}). They occur in a period
368 where the soil water content decreases and reaches values close to the one observed after the
369 rainfall event. However, when the water content increases again, the fluxes become negligible
370 again. Despite few values a similar behaviour could be observed at day 21 and 22 where a
371 decrease of water content seems to lead to high CO_2 fluxes values.

372 ## 4. Discussion

373 ### 4.1.Soil CO_2 diffusivities

374 During the artificial rainfall event, the increase of soil moisture content impacted CO_2
375 soil gas fluxes. The Figure 10 shows the good accordance between CO_2 fluxes measurements
376 and CO_2 concentration gradients calculated between 0 and 0.4 m depth at the beginning of the
377 CO_2 injection until steady state.

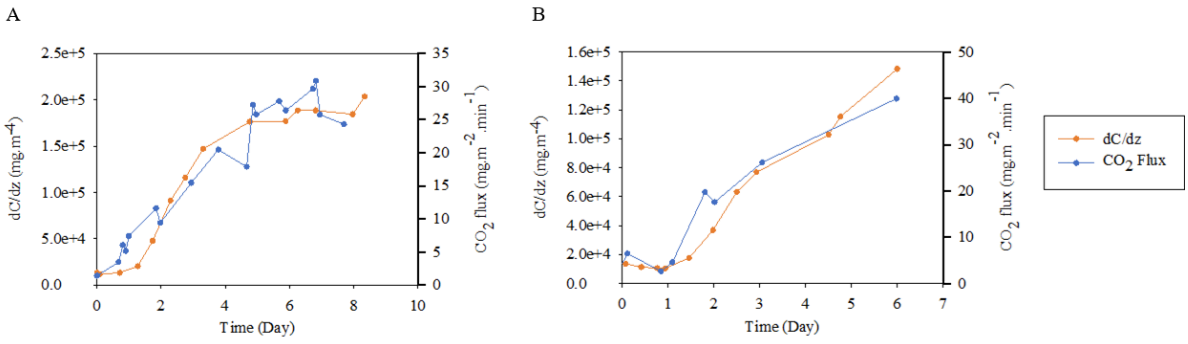


Figure 10. Relationship between CO_2 fluxes measurements and CO_2 concentration gradients (0 - 0.4 m depth) during February experiment (A) and October experiment (B).

378

379 According to first Fick law, the CO_2 flux (F_{CO2}) and CO_2 concentration are related
380 through the effective diffusion coefficient (D_e):

$$F = De \times \frac{dC}{dz} \quad (6)$$

Even if atmospheric pressure varied during the experiments, Atteia and Höhener (2010) showed that advective fluxes play a significant role only when the water saturation is very close one, which never occur during the experiment.

Therefore, the experimental D_e can be calculated using eq. 6 and results from Figure 10. For both experiment, D_e was calculated at steady state (8.5 and 6.0 d) and after the rainfall event (9.22 and 6.17 d) on the first 40 centimetres (Table 3). The experimental D_e were compared to the one predicted by classical empirical formulae in Table 3. Indeed, D_e can be estimated with the molecular diffusivity of CO_2 in air and an empirical tortuosity factors (τ) which was determined in function of gas-phase (Θ_g) and total (Θ) porosity. τ was estimated according to the relationships of Moldrup (2000) $\tau = \Theta_g^{2.5}/\Theta$, Millington and Quirk (1961) $\tau = \Theta_g^{10/3}/\Theta^2$, Millington (1959) $\tau = \Theta_g^{7/3}/\Theta^2$ and Penman (1940) $\tau = 0.66 \times \theta_g$. These calculations were based on the experimental measurements (Figure 3).

Table 3. Effect of soil air-filled porosity on the measured effective diffusion coefficient and comparison with values calculated by empirical methods.

Experiment		1st		2nd	
		At steady state	After artificial rainfall event	At steady state	After artificial rainfall event
Soil moisture content (0 to 0.4 m depth) (-)		0.09	0.24	0.13	0.245
Experimental D_e ($m^2 s^{-1}$)		$2.35x10^{-6} \pm 2.4x10^{-7}$	$9.48x10^{-7} \pm 9.7x10^{-8}$	$4.66x10^{-6} \pm 4.8x10^{-7}$	$9.30x10^{-8} \pm 9.5x10^{-9}$
Estimated D_e[a] ($m^2 s^{-1}$)	Moldrup et al. (2000)	$1.19x10^{-6}$	$2.57x10^{-7}$	$7.53x10^{-7}$	$8.87x10^{-8}$
	Millington and Quirk (1961)	$1.1x10^{-6}$	$4.17x10^{-8}$	$5.97x10^{-7}$	$3.45x10^{-8}$
	Millington (1959)	$4.57x10^{-6}$	$4.63x10^{-7}$	$2.99x10^{-6}$	$4.05x10^{-7}$
	Penman (1940)	$2.20x10^{-6}$	$8.26x10^{-7}$	$1.83x10^{-6}$	$7.80x10^{-7}$

[a] Free-air diffusion coefficient used for calculation were D_{air} CO_2 = $1.39x10^{-5}$ $m^2 s^{-1}$(Pritchard and Currie, 1982)

As expected, D_e decreases with the increase of soil moisture content (Hers et al., 2000; Jassal et al., 2005). According to the 1st experiment results, at steady state (8.5 and 6 d), D_e was

about 2.35×10^{-6} m^2 s^{-1} and decreased drastically after the artificial rainfall event (9.22 d) to 9.48×10^{-7} m^2 s^{-1}. The same observation can be done for the 2nd experiment.

Overall, the comparisons between experimental and calculated D_e indicate that the Penman and Millington (1959) relationships provide correct estimates. Indeed, the D_e were similar or close by a factor of 0.55 to 2.55.

An exception was found for the estimated D_e, during the second experiment (after artificial rainfall event), where the estimated D_e calculated with the Moldrup relationship seemed approaching to experimental value with D_e of 8.87×10^{-8} m^2 s^{-1} and 9.30×10^{-8} m^2 s^{-1}, respectively.

Hers et al. (2000) also observed a difference of the same order of magnitude between the measured and predicted values. They obtained a good comparison between the measured gas-phase tortuosity factor and the one predicted using the Millington and Quirk relationship with measured tortuosity factors about twice the predicted values.

These differences could be partly explained by the uncertainties in the experimental measures on the CO_2 flux, soil moisture contents and soil CO_2 concentrations.

4.2.Influence of rainfall events

Few studies, to our knowledge, tried understanding the impacts of rainfall events on the CO_2 leakages to the environment and more particularly their influence on the CO_2 diffusion along soil profile and CO_2 fluxes (Oh et al., 2019; Seo et al., 2020). Understanding mechanisms is however crucial to advance modelling approaches to simulate CO_2 flux surfaces under changing environmental conditions.

4.2.1. Artificial rainfall event

After the artificial rainfall events, soil moisture content firstly increased while a significant decrease of soil CO_2 concentrations and CO_2 fluxes was observed. After this, CO_2

concentrations and soil water contents reached back the steady state values at approximately 2 days. The recovery process was longer for CO_2 fluxes. However, for both experiments, the return to the steady state of CO_2 fluxes was not observed. During the 1st experiment, it is possible that the measurement was stopped before the end of the recovery step. For the 2nd experiment, the heavy natural rainfall prevented the observation of the return to steady state.

A similar behaviour was observed by Lewicki et al. (2009) and Tommasone Pascale al. (2015). During a CO_2 release experiment, Lewicki et al. (2009) observed a decrease of CO_2 concentration which could have been partially due to changes in soil physical properties associated with significant rainfall events (10 – 20 mm). However, this effect of precipitations was not observed on the CO_2 fluxes. Tommasone Pascale al. (2015) studied the effect of rainstorm events on ^{222}Rn activity in soil, and observed an immediate drop in ^{222}Rn activities by several orders of magnitude after rainfall events. At the end of precipitation, soil ^{222}Rn activities did not appear to recover rapidly, at least for a time span of about a couple of days after storm ending. Tommasone Pascale et al (2015) shared the hypothesis given by Garcia-Vindas and Monnin (2005) stating that the immediate drop in ^{222}Rn activities following rainfall events are attributed to the dissolution of ^{222}Rn into the infiltrated water. This step consists in the "wash-out step" during which rainfall water infiltrates into the pore network and progressively washes out the radon, likely transferring to lower levels of the profile. Besides the different chemical behaviour of ^{222}Rn and CO_2 (e.g. production and decay), the present study seems to support this hypothesis. Indeed, a clear decrease of the total CO_2 mass was observed after the artificial rainfall event (Table 1).

In the mass balance calculations, the loss of CO_2 in the considered volume was like the loss measured at the soil surface. This implies that there is no entering flux of CO_2 from the source located below 80 cm while it is still providing a flux of CO_2. One potential explanation, which is already cited by Viveiros et al. (2008), is that during a significant rainfall event the

449 soil gas is blocked below the infiltrated water. In that case, there could be a significant advective
450 downward soil gas flux that would prevent the arrival of high CO_2 gas from the source.

451 Concerning the slow recovery stage of gas concentrations, there was no explication or
452 hypothesis established in the literature at our knowledge. The results showed that the CO_2
453 profiles went overall back to steady state after 2.37 days from the beginning of rainfall event
454 for the 1st experiment and 1.87 days for the 2nd experiment (Figure 7). However, observation
455 data indicate that depending on depth CO_2 concentrations were not exactly back to steady state
456 at the same time. For example, during the 1st experiment, CO_2 concentration at 0.8 m depth was
457 back to steady state after about 2.46 and after 4.3 d at 0.4 m depth. The longer of recovery time
458 lag at shallow depth may explain the slow recovery process of CO_2 flux. It would have been
459 interesting to follow the temporal evolution of CO_2 concentrations at different depths between
460 the surface and 0.4 m depth to confirm the time lag effect.

461 #### 4.2.2. Influence of natural rainfall events

462 During the 2nd experiment, different intensities of precipitation impacted CO_2 fluxes
463 differently. The low-amplitude rainfall events and short-lived (estimated at less than 1-2 mm)
464 cause a temporary mere wetting of the first centimetres of the ground surface which does not
465 or barely affects soil CO_2 concentrations and flux. On the contrary, significant rainfall events
466 (higher than 2 mm) appear to produce a clear decrease of CO_2 fluxes, owing by increase of soil
467 moisture content in deeper. Tommasone Pascale et al (2015) also observed the modifications
468 of ^{222}Rn activities deriving from significant rainfall depend on rainfall duration, persistency,
469 and intensity.

470 ## 5. Conclusion

471 The effect of rainfall events on soil gas flux was experimentally studied with lysimeter
472 experiments. Rainfall and soil moisture have caused significant modifications in soil CO_2

concentrations and flux during both experiments. During persistent and significant rainfall, the results clearly show a significant decrease of CO_2 flux to atmosphere induced by rainfall infiltration and consequential wash-out of the CO_2 present in the soil. After rainfall events, the recovery processes of soil CO_2 concentrations and fluxes were found to be very slow after the end of the artificial rainfall. Moreover, it can be expected that the temporal evolution of soil CO_2 concentrations is markedly dependent on the rainfall history of the site (total rainfall intensity, frequency and duration, intervals between rainfall events…) and the soil hydrodynamic properties. It should be noted that these experiments simulated conditions with high CO_2 concentrations like conditions encountered at CO_2 storage sites or petroleum-contaminated sites with high degradation rates. The conclusions can perhaps not be generalized to other sites with low CO_2 concentrations, e.g. in arid climates where water infiltration could stimulate respiration. In the present case, respiration in the vadose zone was assumed to be low and independent on moisture content.

Complementary studies are needed to understand and take into account all parameters that drive CO_2 diffusion along soil profile and CO_2 fluxes at the soil-atmosphere interface. Understanding these mechanisms is crucial in order to advance modelling approaches to predict CO_2 surfaces flux under changing environmental conditions.

Acknowledgement

The authors would like to thank the partner companies of the INNOVASOL consortium which permitted to realize this research project.

496 References

497

498 Atteia, O., Höhener, P., 2010. Semianalytical Model Predicting Transfer of Volatile Pollutants
499 from Groundwater to the Soil Surface. Environ. Sci. Technol. 44, 6228–6232.
500 https://doi.org/10.1021/es903477f
501 Beaubien, S.E., Jones, D.G., Gal, F., Barkwith, A.K.A.P., Braibant, G., Baubron, J.-C., Ciotoli,
502 G., Graziani, S., Lister, T.R., Lombardi, S., Michel, K., Quattrocchi, F., Strutt, M.H.,
503 2013. Monitoring of near-surface gas geochemistry at the Weyburn, Canada, CO2-EOR
504 site, 2001–2011. Int. J. Greenh. Gas Control, The IEAGHG Weyburn-Midale CO2
505 Monitoring and Storage Project 16, S236–S262.
506 https://doi.org/10.1016/j.ijggc.2013.01.013
507 Bekele, D.N., Naidu, R., Chadalavada, S., 2014. Influence of spatial and temporal variability
508 of subsurface soil moisture and temperature on vapour intrusion. Atmos. Environ. 88,
509 14–22. https://doi.org/10.1016/j.atmosenv.2014.01.053
510 Bernardo, C., Vries, D.F. de, 2011. Permanent shallow subsoil CO2 flux chambers for
511 monitoring of onshore CO2 geological storage sites. Int. J. Greenh. Gas Control, The
512 5thTrondheim Conference on CO2 Capture, Transport and Storage 5, 565–570.
513 https://doi.org/10.1016/j.ijggc.2010.05.011
514 Bornemann, F., 1920. Kohlensäure und Pflanzenwachstum. Mitt. Dtsch. Landwirtsch.-Ges.
515 35:363.
516 Choi, J.-W., Smith, J.A., 2005. Geoenvironmental Factors Affecting Organic Vapor Advection
517 and Diffusion Fluxes from the Unsaturated Zone to the Atmosphere under Natural
518 Conditions. Environ. Eng. Sci. 22, 95–108. https://doi.org/10.1089/ees.2005.22.95
519 Conant, B.H., Gillham, R.W., Mendoza, C.A., 1996. Vapor Transport of Trichloroethylene in
520 the Unsaturated Zone: Field and Numerical Modeling Investigations.
521 https://doi.org/10.1029/95WR02965
522 Cotel, S., Schaefer, G., Sylvie, T., Marzougui-Jaafar, S., Gay, G., Razakarisoa, O., 2015.
523 Evaluation of VOC fluxes at the soil-air interface using different flux chambers and a
524 quasi-analytical approach. Water. Air. Soil Pollut. 226. https://doi.org/10.1007/s11270-
525 015-2596-y
526 Elío, J., Nisi, B., Ortega, M.F., Mazadiego, L.F., Vaselli, O., Grandia, F., 2013. CO2 soil flux
527 baseline at the technological development plant for CO2 injection at Hontomin (Burgos,
528 Spain). Int. J. Greenh. Gas Control 18, 224–236.
529 https://doi.org/10.1016/j.ijggc.2013.07.013
530 Elío, J., Ortega, M.F., Nisi, B., Mazadiego, L.F., Vaselli, O., Caballero, J., Chacón, E., 2016. A
531 multi-statistical approach for estimating the total output of CO2 from diffuse soil
532 degassing by the accumulation chamber method. Int. J. Greenh. Gas Control 47, 351–
533 363. https://doi.org/10.1016/j.ijggc.2016.02.012
534 Fa, K.-Y., Liu, J.-B., Zhang, Y.-Q., Wu, B., Qin, S.-G., Feng, W., Lai, Z.-R., 2015. CO2
535 absorption of sandy soil induced by rainfall pulses in a desert ecosystem. Hydrol.
536 Process. 29, 2043–2051. https://doi.org/10.1002/hyp.10350
537 Garcia-Vindas, J.R., Monnin, M.M., 2005. Radon concentration measurements in the presence
538 of water and its consequences for Earth sciences studies. Radiat. Meas. 39, 319–322.
539 https://doi.org/10.1016/j.radmeas.2004.06.014
540 Hers, I., Li, L., Hannam, S., 2004. Evaluation of soil gas sampling and analysis techniques at a
541 former petrochemical plant site. Environ. Technol. 25, 847–860.
542 https://doi.org/10.1080/09593330.2004.9619377

Hers, I., Zapf-Gilje, R., Li, L., Atwater, J., 2000. Measurement of in Situ Gas-Phase Diffusion Coefficients. Environ. Technol. 21, 631–640. https://doi.org/10.1080/09593330.2000.9618948

Jassal, R., Black, A., Novak, M., Morgenstern, K., Nesic, Z., Gaumont-Guay, D., 2005. Relationship between soil CO2 concentrations and forest-floor CO2 effluxes. Agric. For. Meteorol. 130, 176–192. https://doi.org/10.1016/j.agrformet.2005.03.005

Kim, J., Yu, S., Yun, S.-T., Kim, K.-H., Kim, J.-H., Shinn, Y.-J., Chae, G., 2019. CO2 leakage detection in the near-surface above natural CO2-rich water aquifer using soil gas monitoring. Int. J. Greenh. Gas Control 88, 261–271. https://doi.org/10.1016/j.ijggc.2019.06.015

Klenbusch, M., 1986. Measurement of Gaseous Emission Rates From Land Surfaces Using an Emission Isolation Flux Chamber: User's Guide. US Environ. Prot. Agency Wash. DC EPA6008-86008.

Lelli, M., Raco, B., 2017. A reliable and effective methodology to monitor CO2 flux from soil: The case of Lipari Island (Sicily, Italy). Appl. Geochem. 85, 73–85. https://doi.org/10.1016/j.apgeochem.2017.08.004

Lewicki, J.L., Hilley, G.E., Dobeck, L., Spangler, L., 2009. Dynamics of CO2 fluxes and concentrations during a shallow subsurface CO2 release. Environ. Earth Sci.

Ma, J., Zheng, X.-J., Li, Y., 2012. The response of CO2 flux to rain pulses at a saline desert. Hydrol. Process. 26, 4029–4037. https://doi.org/10.1002/hyp.9204

Matthias, A.D., Blackmer, A.M., Bremner, J.M., 1980. A Simple Chamber Technique for Field Measurement of Emissions of Nitrous Oxide from Soils. J. Environ. Qual. 9, 251–256. https://doi.org/10.2134/jeq1980.00472425000900020017x

Millington, R.J., 1959. Gas Diffusion in Porous Media. Science 130, 100–102. https://doi.org/10.1126/science.130.3367.100-a

Millington, R.J., Quirk, J.P., 1961. Permeability of porous solids. Trans. Faraday Soc. 57, 1200–1207. https://doi.org/10.1039/TF9615701200

Moldrup, P., Olesen, T., Gamst, J., Schjønning, P., Yamaguchi, T., Rolston, D.E., 2000. Predicting the Gas Diffusion Coefficient in Repacked Soil Water-Induced Linear Reduction Model. Soil Sci. Soc. Am. J. 64, 1588–1594. https://doi.org/10.2136/sssaj2000.6451588x

Norman, J.M., Kucharik, C.J., Gower, S.T., Baldocchi, D.D., Crill, P.M., Rayment, M., Savage, K., Striegl, R.G., 1997. A comparison of six methods for measuring soil-surface carbon dioxide fluxes. J. Geophys. Res. Atmospheres 102, 28771–28777. https://doi.org/10.1029/97JD01440

Oh, Y.Y., Yun, S.T., Yu, S., Kim, H.J., Jun, S.C., 2019. A novel wavelet-based approach to characterize dynamic environmental factors controlling short-term soil surface CO2 flux: Application to a controlled CO2 release test site (EIT) in South Korea. Geoderma 337, 76–90. https://doi.org/10.1016/j.geoderma.2018.09.017

Palaia, T., Jimmo, A., Mahler, N., Molinari, C., Clements, L., 2018. Technical measurement guidance for LNAPL natural source zone depletion. CRC CARE Tech. Rep. No 44 254. https://doi.org/10.1089/ees.2005.22.95

Penman, H.L., 1940. Gas and vapour movements in the soil: I. The diffusion of vapours through porous solids. J. Agric. Sci. 30, 437–462. https://doi.org/10.1017/S0021859600048164

Petersen, L.W. (Danish I. of P. and S.S., El-Farhan, Y.H., Moldrup, P., Rolston, D.E., Yamaguchi, T., 1996. Transient diffusion, adsorption, and emission of volatile organic vapors in soils with fluctuating low water contents. J. Environ. Qual. USA.

Reinhart, D.R., Cooper, D.C., Walker, B.L., 1992. Flux Chamber Design and Operation for the Measurement of Municipal Solid Waste Landfill Gas Emission Rates. J. Air Waste Manag. Assoc. 42, 1067–1070. https://doi.org/10.1080/10473289.1992.10467053

Risk, D.A., Kellman, L.M., Beltrami, H., 2002. Soil CO2 production and surface flux at four climate observatories in eastern Canada. https://doi.org/10.1029/2001GB001831
Rochette, P., Hutchinson, G., 2005. Measurement of Soil Respiration in situ: Chamber Techniques. Publ. USDA-ARS UNL Fac.
Rodier, J., 1976. L'analyse de l'eau. Eaux naturelles, eaux résiduaires, eaux de mer., Dunod Tech, Bordas, Paris. ed.
Sander, S.P., Friedl, R.R., Barker, J.R., Abbatt, J.P.D., Burkholder, J.B., Friedl, R.R., Golden, D.M., Huie, R.E., Kolb, C.E., Kurylo, M.J., Moortgat, G.K., Orkin, V.L., Wine, P.H., 2011. Chemical Kinetics and Photochemical Data for Use in Atmospheric Studies Evaluation No. 17. JPL Publ. 10–6, Jet Propulsion Laboratory, Pasadena, 684.
Schroder, I.F., Zhang, H., Zhang, C., Feitz, A.J., 2016. The role of soil flux and soil gas monitoring in the characterisation of a CO2 surface leak: A case study in Qinghai, China. Int. J. Greenh. Gas Control 54, 84–95. https://doi.org/10.1016/j.ijggc.2016.07.030
Seo, D.H., Han, W.S., Park, E., Jeong, J., Oh, Y.-Y., Kim, H.-J., Yoo, G., Jun, S.-C., Yun, S.-T., 2020. Analyses and numerical evaluation of integrated time-series monitoring datasets including CO2 concentration and fluxes at controlled CO2 release site in South Korea. J. Hydrol. 590, 125213. https://doi.org/10.1016/j.jhydrol.2020.125213
Shao, H., Ussiri, D.A.N., Patterson, C.G., Locke, R.A., II, Wang, H., Taylor, A.H., Cohen, H.F., 2019. Soil gas monitoring at the Illinois Basin – Decatur Project carbon sequestration site. Int. J. Greenh. Gas Control 86, 112–124. https://doi.org/10.1016/j.ijggc.2019.04.012
Shen, R., Pennell, K.G., Suuberg, E.M., 2013. Influence of Soil Moisture on Soil Gas Vapor Concentration for Vapor Intrusion. Environ. Eng. Sci. 30, 628–637. https://doi.org/10.1089/ees.2013.0133
Shen, R., Pennell, K.G., Suuberg, E.M., 2012. A numerical investigation of vapor intrusion--the dynamic response of contaminant vapors to rainfall events. Sci. Total Environ. 437, 110–120. https://doi.org/10.1016/j.scitotenv.2012.07.054
Smith, J.A., Tisdale, A.K., Cho, H.J., 1996. Quantification of Natural Vapor Fluxes of Trichloroethene in the Unsaturated Zone at Picatinny Arsenal, New Jersey. Environ. Sci. Technol. 30, 2243–2250. https://doi.org/10.1021/es950610c
Tillman, F.D., Smith, J.A., 2004. Design and laboratory testing of a chamber device to measure total flux of volatile organic compounds from the unsaturated zone under natural conditions. J. Contam. Hydrol. 75, 71–90. https://doi.org/10.1016/j.jconhyd.2004.04.005
Tommasone Pascale, F., Carbone, P., De Francesco, S., Cuoco, E., Tedesco, D., 2015. Rainstorm-induced soil 222Rn concentration spikes observed in Southern Italy. Environ. Earth Sci. 73, 8177–8187. https://doi.org/10.1007/s12665-014-3976-0
Viveiros, F., Ferreira, T., Cabral Vieira, J., Silva, C., Gaspar, J.L., 2008. Environmental influences on soil CO2 degassing at Furnas and Fogo volcanoes (São Miguel Island, Azores archipelago). J. Volcanol. Geotherm. Res., Volcanic Flows and Falls 177, 883–893. https://doi.org/10.1016/j.jvolgeores.2008.07.005
Werner, D., Grathwohl, P., Höhener, P., 2004. Review of Field Methods for the Determination of the Tortuosity and Effective Gas-Phase Diffusivity in the Vadose Zone. Vadose Zone J. 3, 1240–1248. https://doi.org/10.2136/vzj2004.1240
Wilke, B.-M., 2005. Determination of Chemical and Physical Soil Properties, in: Margesin, R., Schinner, F. (Eds.), Monitoring and Assessing Soil Bioremediation, Soil Biology. Springer, Berlin, Heidelberg, pp. 47–95. https://doi.org/10.1007/3-540-28904-6_2
Yang, L., Chen, Z., Zhang, X., Liu, Y., Xie, Y., 2015. Comparison study of landfill gas emissions from subtropical landfill with various phases: A case study in Wuhan, China.

643 J. Air Waste Manag. Assoc. 65, 980–986.
644 https://doi.org/10.1080/10962247.2015.1051605
645